Journal of Zhejiang University-SCIENCE C (Computers & Electronics)
ISSN 1869-1951 (Print); ISSN 1869-196X (Online)
www.zju.edu.cn/jzus; www.springerlink.com
E-mail: jzus@zju.edu.cn

Analysis, design, and experimental evaluation of power calculation in digital droop-controlled parallel microgrid inverters*

Ming-zhi GAO[1], Min CHEN[†‡1], Cheng JIN[1], Josep M. GUERRERO[2], Zhao-ming QIAN[1]

([1]*Department of Applied Electronics, Zhejiang University, Hangzhou 310027, China*)

([2]*Institute of Energy Technology, Aalborg University, Aalborg 9000, Denmark*)

[†]E-mail: calim@zju.edu.cn

Received Aug. 8, 2012; Revision accepted Nov. 1, 2012; Crosschecked Dec. 23, 2012

Abstract: Parallel operation of distributed generation is an important topic for microgrids, which can provide a highly reliable electric supply service and good power quality to end customers when the utility is unavailable. However, there is a well-known limitation: the power sharing accuracy between distributed generators in a parallel operation. Frequency and voltage droop is a well-established control method for improving power sharing performance. In this method, the active and reactive power calculations are used to adjust the frequency and amplitude of the output voltage. This paper describes the digital implementation of a droop method, and analyzes the influence of power calculation on droop method performance. According to the analysis, the performance of droop control in a digital control system is limited by the accuracy and speed of the power calculation method. We propose an improved power calculation method based on *p-q* theory to improve the performance of the droop control method, and we compare our new method with two traditional power calculation methods. Finally, simulation results and experimental results from a three single-phase 1-kW-inverter system are presented, which validate the performance of our proposed method.

Key words: Distributed generators, Distributed energy storages, Microgrid, Wireless parallel, Droop control, Digital control system, *p-q* theory

doi:10.1631/jzus.C1200236 **Document code:** A **CLC number:** TM464

1 Introduction

Microgrids are defined as systems that have at least one distributed energy resource (DER) and associated loads, which can form intentional islands in electrical distribution systems and provide higher reliability electric service and better power quality to the end customers independently compared with the traditional utility (Kroposki *et al*., 2008). In general, a microgrid comprises distributed generators (DGs), distributed energy storages (DSs), and local loads (Ahn *et al*., 2010). This concept allows for the integration of renewable and non-conventional energy resources through different kinds of DGs, such as photovoltaic panels, fuel cells (FCs), or wind turbines (Hatziargyriou *et al*., 2007; Guerrero *et al*., 2010).

A microgrid can be thought of as a controllable subsystem of a utility, and should operate safely and reliably in grid-connected mode and in islanding mode (de Brabandere *et al*., 2007; Guerrero *et al*., 2008; 2009). When the microgrid connects to the utility, DGs are able to maintain a constant output power regardless of the load variation, because the power mismatch can be compensated by the grid (Ahn *et al*., 2010). However, during islanding mode, DGs and DSs working in parallel operation must keep the local voltage stable, match customers' requirements exactly, provide (or absorb) the instantaneous power to the customers, and protect the internal microgrid (Kroposki *et al*., 2008). At the same time, every DG or DS should share output active and reactive power with other units in exact accordance with

‡ Corresponding author

* Project (No. 51107116) supported by the National Nature Science Foundation of China

the load, to avoid circulating currents (Guerrero *et al*., 2008).

Many control techniques have been introduced to achieve power sharing in parallel operation. A well-established control method is the droop method (Sun *et al*., 2003; Guerrero *et al*., 2005; Roslan *et al*., 2011). This technique adjusts the frequency and amplitude of output voltage to compensate for active and reactive power unbalances. Many researchers have focused on improving the droop control, and many improved methods have been proposed, such as the modified droop (Chiang *et al*., 2001; Barklund *et al*., 2008; Diaz *et al*., 2010; Majumder *et al*., 2010), virtual impedance loops (Guerrero *et al*., 2006; Matas *et al*., 2010; He and Li, 2011; Yao *et al*., 2011), combined droop (Marwali *et al*., 2004; Golestan *et al*., 2009; Chung *et al*., 2010; Hasanzadeh *et al*., 2010), and adaptive droop (Yang *et al*., 2006; Mohamed and El-Saadany, 2008; Li and Kao, 2009; Rokrok and Golshan, 2010) control schemes.

In the droop method, active power and reactive power calculations are the foundation which is used to adjust the frequency and amplitude of the output voltage. Nearly all droop methods employ various complicated algorithms realized in digital control systems to improve the power sharing performance. To obtain better transient performance, these control methods need to adjust the frequency and amplitude in every switching frequency through the digital control system. A highly accurate and fast power calculation method is required to ensure that the control method can obtain the optimal correction value. Therefore, droop performance is limited by the accuracy and speed of the power calculation in a digital control system.

In this paper, we analyze the influence of the power calculation method on parallel performance by theoretical derivation, and show that the accuracy and speed of the power calculation are important for the performance of a parallel operation. However, traditional power calculation methods have a slow and oscillating transient response due to a low pass filter (LPF) and average computing cycle, and could be easily influenced by disturbance and variation in load, such as non-linear or light load (Ren *et al*., 2010; Yao *et al*., 2010).

Thus, in this paper, we try to solve the problems of load sharing performance by improving the power calculation method. A preferable power calculation based on a modified *p-q* theory is proposed to solve the problem and improve dynamic performance. An instantaneous active and reactive power (*p-q*) theory has been proposed for three-phase circuit applications (Afonso *et al*., 2003; Aredes *et al*., 2009). Although the *p-q* theory, in its original concept, was conceived to be used in three-phase systems, it is possible to implement it in single-phase systems using some modifications (Oliveira da Silva *et al*., 2008).

2 Droop control method overview

Fig. 1 depicts the structure of a microgrid comprising various units, such as DGs, DSs, and local loads. These units are connected through an AC common bus (Kroposki *et al*., 2008). The equivalent circuit of a DG or DS in a parallel operation can be described in Fig. 2 (Yao *et al*., 2010). The apparent power delivered to the load is shown as

$$\boldsymbol{S} = P + \mathrm{j}Q = \boldsymbol{E} \cdot \boldsymbol{I}_{\mathrm{o}}^{*} = E\angle\phi \cdot \left(\frac{E\angle\phi - V\angle 0}{Z\angle\theta} \right)^{*}. \quad (1)$$

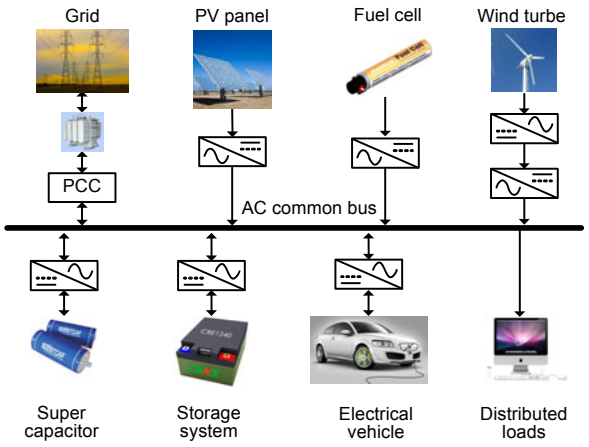

Fig. 1 Structure of a microgrid
PV: Photovoltaic; PCC: point of common coupling

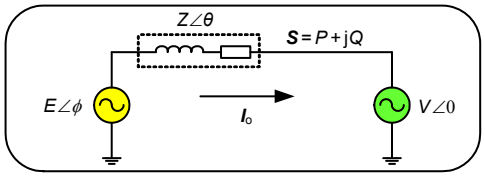

Fig. 2 Equivalent circuit of a distributed generator (Yao *et al*., 2010)

The active power P and reactive power Q injected to the bus by each unit can be expressed as (Guerrero *et al*., 2006)

$$\begin{cases} P=\left(\dfrac{EV}{Z}\cos\phi-\dfrac{V^2}{Z}\right)\cos\theta+\dfrac{EV}{Z}\sin\phi\sin\theta, \\ Q=\left(\dfrac{EV}{Z}\cos\phi-\dfrac{V^2}{Z}\right)\sin\theta-\dfrac{EV}{Z}\sin\phi\cos\theta, \end{cases} \tag{2}$$

where E and V are the amplitudes of the DG output voltage v_o and the common bus voltage v_{bus}, respectively, ϕ is the power angle, and Z and θ are the magnitude and phase of the output impedance, respectively. Note that both P and Q depend simultaneously on the output voltage phase ϕ and the amplitude E.

The line impedance angle θ largely determines the droop control law (Guerrero *et al*., 2006). Traditionally, the inverter line impedance is considered to be inductive (Guerrero *et al*., 2008), due to the use of an output inductor used to balance the output current and restrain the instantaneous circulating current. When θ is 90°, Eq. (3) can be obtained from Eq. (2):

$$\begin{cases} P=\dfrac{EV}{Z}\sin\phi\approx\dfrac{EV}{Z}\phi, \\ Q=\dfrac{EV\cos\phi-V^2}{Z}\approx\dfrac{V}{Z}(E-V). \end{cases} \tag{3}$$

Hence, it is clear that if the angle difference ϕ is small, the real power can be controlled by controlling ϕ, while the reactive power can be controlled by controlling E.

Using the droop method, each unit uses frequency instead of phase to control the active power flows, considering that they do not know the initial phase values of the other units. Therefore, the droop control method can be expressed in a general form as

$$\begin{cases} \omega=\omega^*-mP, \\ E=E^*-nQ. \end{cases} \tag{4}$$

The higher are the droop coefficients, the better is the power sharing. However, the frequency and amplitude regulation deteriorate (Fig. 3). Thus, this tradeoff must be considered in these two droop equations.

3 Performance limitations of the digital droop method

Nowadays, digital control is widely used in power electronic systems to realize complex control algorithms and to improve performance. Fig. 4 shows the structure of DGs with a digital control system in parallel operation. Table 1 shows the nomenclature of the parameters. The yellow part in Fig. 4 is the traditional double-loop control and the blue part is the droop method. The yellow and blue parts are both realized in the digital control system and should be described in Z-domain. The zero-order hold (ZOH) and LC filter, shown in orange, should be described in S-domain.

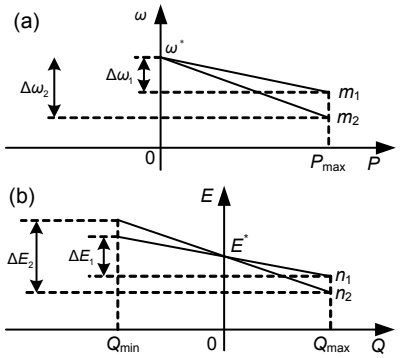

Fig. 3 Static droop characteristics
(a) P-ω droop control; (b) Q-V droop control

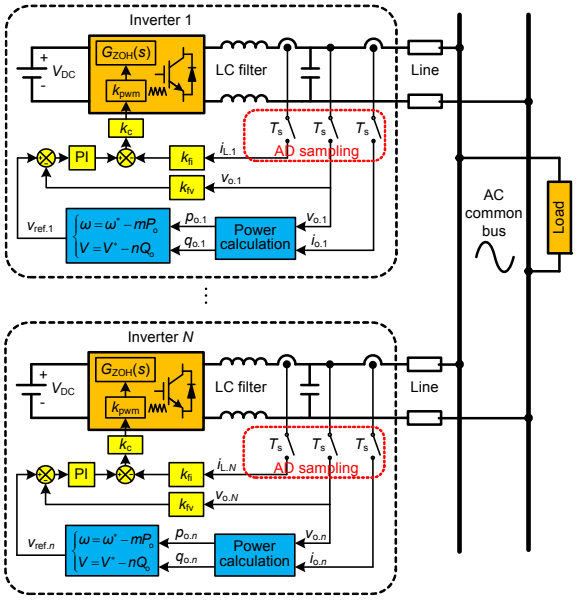

Fig. 4 Structure of DGs with a digital control system
Yellow part: traditional double-loop control; blue part: droop method; orange part: zero-order hold (ZOH) and LC filter. References to color refer to the online version of this figure

Table 1 Nomenclature of control parameters

Parameter	Description
k_p	Proportionality coefficient of proportional-integral control (PI)
k_i	Integral coefficient of PI
k_{fv}	Feedback coefficient of voltage loop
k_{fi}	Feedback coefficient of current loop
k_c	Gain of current inner loop
k_{pwm}	Equivalent gain of inverter
L_f	Inductance of LC filter
C_f	Capacitance of LC filter
X_{load}	Impedance of inverter's load

The droop method generates a reference voltage v_{ref}, according to the active and reactive power. Traditional double-loop control comprises the instantaneous voltage outer loop and the current inner loop, and can guarantee the output voltage v_o follows the reference voltage robustly. The closed transfer function of the double-loop control is shown as

$$\frac{V_o(z)}{V_{ref}(z)}=k_c\left(1-\frac{1}{z}\right)\frac{G_1(s)}{s}G_{PI}(z)\cdot\left[1+k_c\left(1-\frac{1}{z}\right)\cdot Z\left(\frac{G_1T_1(s)}{s}\right)+k_ck_{fv}\left(1-\frac{1}{z}\right)Z\left(\frac{G_1(s)}{s}\right)G_{PI}(z)\right]^{-1}, \tag{5}$$

where $V_{ref}(z)$ and $V_o(z)$ are the discretized expressions of v_{ref} and v_o, respectively. $G_1(s)$, $G_1T_1(s)$, $G_{ZOH}(s)$, and $G_{PI}(z)$ are shown as Eqs. (6)–(9), respectively:

$$G_1(s)=\frac{k_{pwm}X_{load}}{s^2L_fCX_{load}+sL_f+X_{load}}, \tag{6}$$

$$G_1T_1(s)=\frac{k_{fi}k_{pwm}(sCX_{load}+1)}{s^2L_fCX_{load}+sL_f+X_{load}}, \tag{7}$$

$$G_{ZOH}(s)=\frac{1-e^{-Ts}}{s}, \tag{8}$$

$$G_{PI}(z)=k_p+\frac{k_iT_s}{1-z^{-1}}. \tag{9}$$

In the droop method, the angular frequency and amplitude of the output voltage are adjusted to realize power sharing. To obtain better transient performance, the droop control needs to adjust the frequency and amplitude in every switching frequency via the digital control system. Thus, an accurate and highly-efficient execution mechanism for the droop method is very important for parallel operation performance. According to Eq. (4), the control accuracy of the droop method can be obtained as

$$\begin{cases}|\delta P|=\dfrac{2\pi}{m}|\delta f_o|,\\ |\delta Q|=\dfrac{1}{n}|\delta E|,\end{cases} \tag{10}$$

where $f_o=\omega/(2\pi)$. Therefore, the droop performance is impacted by the values of the droop parameters (m and n) and the control precision (δf_o and δE) of the digital system (Fig. 5).

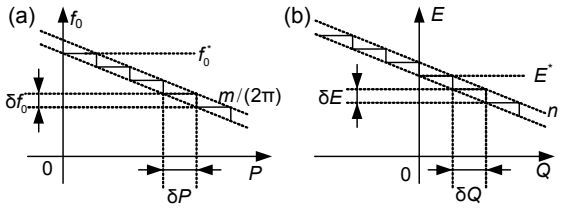

Fig. 5 Droop performance with control precision
(a) P-ω droop control; (b) Q-V droop control

3.1 Digital implementation of the *Q*-*V* droop method

In a digital system, the control precision of Q-V droop is determined mainly by the N-bit A/D sampling precision. If the output voltage v_o is described by $E\sin(\omega t)$, then δE can be obtained as

$$|\delta E|=\frac{2E}{2^N}. \tag{11}$$

For instance, if n is set as 0.0001 V/var (which means every 1000 var reactive power causes output voltage to change by 0.1 V), N=12, and E=155 V, then δQ=7.6 W according to Eqs. (10) and (11). That is, if the variation in reactive power is smaller than 7.6 W, the output voltage remains unchanged.

3.2 Digital implementation of the *P*-ω droop method

The realization of the P-ω droop is more complex than the Q-V droop. Take the DSP F2808 for example. Fig. 6 shows the relationship between the inverter's output frequency f_o, the switching frequency f_s ($1/T_s$), and the DSP's oscillator frequency f_{osc} ($1/T_{osc}$). N_{tri} is an adjustable parameter in DSP. Thus, the relationship between f_o, f_s, and f_{osc} can be described by

$$\begin{cases} f_{\mathrm{o}} = f_{\mathrm{osc}} /(2L_N N_{\mathrm{tri}}), \\ f_{\mathrm{s}} = L_N f_{\mathrm{o}}. \end{cases} \tag{12}$$

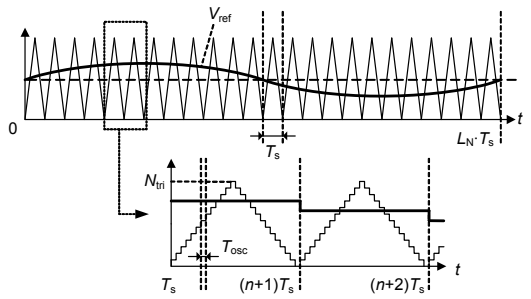

Fig. 6 Relationship between the inverter's output frequency f_o, the switching frequency f_s ($1/T_s$), and the DSP's oscillator frequency f_{osc}

According to Eq. (5), v_o is controlled by v_{ref}, and v_{ref} is implemented by the DSP's fixed interrupt, and can be described by

$$\begin{cases} V_{\mathrm{ref}}(kT_{\mathrm{s}}) = \sin\big(\theta(k)\big), \\ \theta(k) = \theta(k-1) + 2\pi / L_{\mathrm{N}}, \end{cases} \tag{13}$$

where L_N is the table length of the reference voltage.

Hence, combining Eqs. (12) and (13), there are two solutions to realize a change in output frequency. One is by changing T_s, which can be implemented by changing N_{tri}, and the other is by changing L_N.

In the first solution, L_N is fixed, and thus the reference voltage can be obtained by using a look-up table. This solution is very easy to implement and can avoid complicated sinusoidal calculations, thus saving DSP resource.

After discretizing Eq. (12), Eq. (14) can be obtained as follows:

$$\left|\delta f_{\mathrm{o}}\right| = \frac{f_{\mathrm{osc}}}{2L_{\mathrm{N}} N_{\mathrm{tri}}^2}\left|\delta N_{\mathrm{tri}}\right|. \tag{14}$$

In the digital system, δN_{tri}=1. According to Eqs. (10) and (14), Eq. (15) can be obtained as follows:

$$\left|\delta P\right| = \frac{\pi f_{\mathrm{osc}}}{mL_{\mathrm{N}} N_{\mathrm{tri}}^2}\left|\delta N_{\mathrm{tri}}\right|. \tag{15}$$

For instance, in DSP F2808 with f_{osc}=100 MHz, f_o=50 Hz, and f_s is chosen as 20 kHz, then N=400 and N_{tri}=2500. For a 1-kW inverter, if the parameter m is set as $2\pi/10\,000$, every 1000 W of active power changes by 0.1 Hz. In the non-load, f_o=50 Hz and N_{tri}=2500, thus δP=199.2 W. In the full load, f_o= 49.9 Hz and N_{tri}=2505, thus δP=200 W. As an approximation, it can be assumed that every 200 W of active power causes N_{tri} to change by 1. Moreover, if the parameter m increases, δP will decrease due to Eq. (15), but the system stability will be weak.

In the second solution, the frequency variation can be realized by adjusting L_N, so that the control precision is highly affected by the computational accuracy of the sinusoidal function. However, the second solution has a high computational cost. The reference voltage should be re-evaluated in every switching period T_s through the sinusoidal function. When the switching frequency is very high, the complex instruction cycles of the sinusoidal function will be a very big burden for a digital system.

To address some of these problems, we analyzed the control precision of droop realization in a digital system. According to Eq. (10), the bigger is the droop parameter, the higher is the control precision of the droop method, but the system stability will be worse. The digital implementation of the droop method constrains the effect of the droop parameters.

The influence of the power calculation also needs to be considered in the design of droop parameters. If the ripple of the power calculation result is bigger than the control precision of the droop method, or if the speed of the power calculation is much slower than the control system, the droop parameters will fail to control the system and the stability will deteriorate. Thus, the accuracy and speed of the power calculation, analyzed in the next section, are very important for the performance of a parallel operation.

4 Review and comparisons of power calculation methods

When using the droop method, every paralleled inverter works as a voltage source, and its harmonics are usually small. However, the output current i_o of the inverter usually has a large number of odd harmonics, especially when sharing non-linear loads. Thus, v_o and i_o of all the inverters are described as

$$\begin{cases} v_o = \sqrt{2}U_r \sin(\omega t), \\ i_o = \sqrt{2}I_r \sin(\omega t + \theta_1) + \sqrt{2}I_3 \sin(3\omega t + \theta_3) \\ \quad + \sqrt{2}I_5 \sin(5\omega t + \theta_5) + \cdots, \end{cases} \quad (16)$$

where U_r and I_r are the fundamental harmonic effective values of the output voltage and output current, respectively.

Traditional power calculation methods can generally be classified as either product & LPF methods or period average methods. Both types have a slow and oscillating transient response due to LPF and an average computing cycle, and could be easily impacted by a disturbance or variation in load, such as a non-linear or light load. An improved method based on the modified *p-q* theory is proposed in this section and then analyzed and compared with the traditional methods.

4.1 Method 1: product & low pass filter (LPF) method (Guerrero *et al.*, 2004; 2006)

Fig. 7 shows the principle of the product & LPF method. According to Eq. (16), the product of v_o and i_o can be obtained as

$$\begin{aligned} p &= v_o i_o \\ &= 2U_r \sin(\omega t) \cdot [I_r \sin(\omega t + \theta_1) + I_3 \sin(3\omega t + \theta_3) \\ &\quad + I_5 \sin(5\omega t + \theta_5) + \cdots] \\ &= U_r I_r \cos\theta_1 - U_r I_r \cos(2\omega t + \theta_1) + U_r I_3 \cos(2\omega t + \theta_3) \\ &\quad - U_r I_3 \cos(4\omega t + \theta_3) + U_r I_5 \cos(4\omega t + \theta_5) - \cdots, \end{aligned} \quad (17)$$

which is the instantaneous active power. The calculation result includes various harmonics components and DC component $U_r I_r \cos\theta_1$. The DC component equals the value of the average active power P. So active power can be obtained by filtering the product of output voltage v_o and current i_o using LPF.

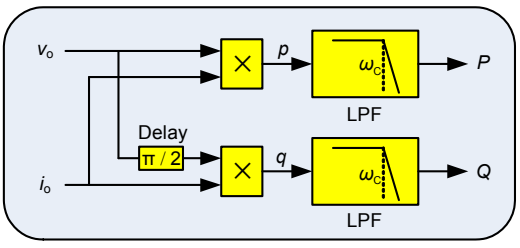

Fig. 7 Principle of method 1

Using a similar method, the average value Q of the reactive power can be obtained by delaying the output voltage of π/2 through a circular buffer, multiplying i_o, and filtering this product using LPF. The product is shown as

$$\begin{aligned} q &= v_o(t - T/4) \cdot i_o(t) \\ &= 2U_r \sin(\omega t - \pi/2) \cdot [I_r \sin(\omega t + \theta_1) \\ &\quad + I_3 \sin(3\omega t + \theta_3) + I_5 \sin(5\omega t + \theta_5) + \cdots] \\ &= U_r I_r \sin\theta_1 - U_r I_r \sin(2\omega t + \theta_1) \\ &\quad + U_r I_3 \sin(2\omega t + \theta_3) - U_r I_3 \sin(4\omega t + \theta_3) \\ &\quad + U_r I_5 \sin(4\omega t + \theta_5) - \cdots. \end{aligned} \quad (18)$$

4.2 Method 2: period-average method (Ren *et al.*, 2010)

This method is based on the definition of average power in Eq. (19):

$$\begin{cases} P = \int_t^{t+T} u(t) i(t) \mathrm{d}t = U_r I_r \cos\theta_1, \\ Q = \int_t^{t+T} u(t - T/4) i(t) \mathrm{d}t = U_r I_r \sin\theta_1. \end{cases} \quad (19)$$

When this method is realized on a digital system, Eq. (20) can be obtained by discretizing Eq. (19):

$$P = \frac{1}{T}\sum_{n=1}^{N} U_s(n) I_s(n) T_s = \frac{1}{N}\sum_{n=1}^{N} U_s(n) I_s(n), \quad (20)$$

where $U_s(n)$ and $I_s(n)$ are the sampling voltage and current, respectively, in a digital system. Thus, the active power value can be obtained by dividing the sum of $U_s(n)I_s(n)$ in a period by N. Therefore, the accuracy is determined by f_s, and the speed is determined by f_o. Moreover, LPF is not needed in this method. In a similar way, the reactive power value can be obtained by delaying the output voltage of π/2 rad, which equals $N/4$ in Eq. (21):

$$Q = \frac{1}{N}\sum_{n=1}^{N} I_s(n) U_s\left(n - \frac{N}{4}\right). \quad (21)$$

4.3 Method 3: the proposed method based on *p-q* theory (Oliveira da Silva *et al.*, 2008)

The *p-q* theory has been widely used in active power filter applications to compensate for reactive

and harmonic powers generated by non-linear loads. Although the *p*-*q* theory, in its original concept, was idealized to be used in three-phase systems, it is possible to implement it in single-phase systems using some modifications (Oliveira da Silva *et al*., 2008).

According to the *p*-*q* theory:

$$\begin{bmatrix} p \\ q \end{bmatrix} = \frac{1}{2}\begin{bmatrix} v_\alpha & v_\beta \\ v_\beta & -v_\alpha \end{bmatrix}\begin{bmatrix} i_\alpha \\ i_\beta \end{bmatrix} = \begin{bmatrix} P \\ Q \end{bmatrix} + \begin{bmatrix} \tilde{p} \\ \tilde{q} \end{bmatrix}, \tag{22}$$

the instantaneous active power p and reactive power q can be obtained. The voltage v_β and current i_β are obtained by introducing a phase delay of π/2 to the output voltage v_α and current i_α.

Substituting Eq. (16) into Eq. (22), we can obtain p and q as

$$\begin{cases} p = U_\mathrm{r} I_\mathrm{r} \cos\theta_1 + U_\mathrm{r} I_3 \cos(2\omega t + \theta_3) \\ \quad + U_\mathrm{r} I_5 \cos(4\omega t + \theta_5) + \cdots, \\ q = U_\mathrm{r} I_\mathrm{r} \sin\theta_1 + U_\mathrm{r} I_3 \sin(2\omega t + \theta_3) \\ \quad + U_\mathrm{r} I_5 \sin(4\omega t + \theta_5) + \cdots. \end{cases} \tag{23}$$

In this method, LPF is also needed to obtain accurate power values of P and Q. A diagram of method 3 is shown in Fig. 8.

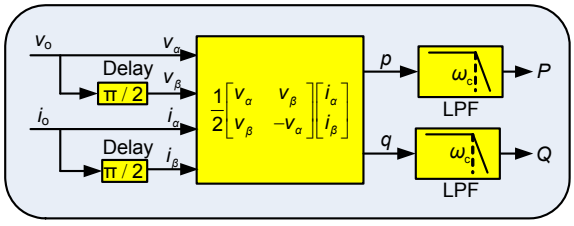

Fig. 8 Principle of the proposed method

4.4 Comparisons

Eq. (24) shows the comparison of the active power results from the above three methods:

$$\begin{cases} p_1 = U_\mathrm{r} I_\mathrm{r} \cos\theta_1 - U_\mathrm{r} I_\mathrm{r} \cos(2\omega t + \theta_1) \\ \quad + U_\mathrm{r} I_3 \cos(2\omega t + \theta_3) - U_\mathrm{r} I_3 \cos(4\omega t + \theta_3) \\ \quad + U_\mathrm{r} I_5 \cos(4\omega t + \theta_5) - \cdots, \\ p_2 = U_\mathrm{r} \cos\theta_1, \quad \text{when } N \to \infty, \\ p_3 = U_\mathrm{r} \cos\theta_1 + U_\mathrm{r} I_3 \cos(2\omega t + \theta_3) \\ \quad + U_\mathrm{r} I_5 \cos(4\omega t + \theta_5) + \cdots, \end{cases} \tag{24}$$

where p_1, p_2, and p_3 express the active power for methods 1, 2, and 3, respectively.

In method 1, the harmonic component of $U_\mathrm{r} I_\mathrm{r} \cos(2\omega t + \theta_1)$ is very close to the DC value, so the cut-off frequency ω_c of LPF should be much lower than the harmonics frequency 2ω, which is usually below 10 rad/s (1.59 Hz) in this study. Thus, the dynamic performance is slowed down sequentially by ω_c.

Method 2 can obtain an accurate power value in a period. An LPF is not needed, because the computing result has only a DC component. However, every calculation needs one line-frequency period of output voltage, so the response is not instantaneous but periodic. Therefore, this method has an unsatisfactory performance, especially when the load is changed suddenly.

In method 3, both the voltage and current should be delayed by π/2 through a circular buffer, which means that more memory space and computing time is needed for implementation on a DSP board.

Similar to method 1, the response of method 3 is instantaneous, and LPF is necessary to obtain an accurate power value. However, in method 3, the harmonics of $\sum_{n=1}^{\infty} U_\mathrm{r} I_{2n-1} (2n\omega t + \theta)$ (I_1=I_r) are all eliminated. I_r is much larger than I_n, so the harmonics of method 3 are much smaller than those of method 1. The cut-off frequency of LPF in method 3 can be higher, and was about 100 rad/s (15.92 Hz) in this experiment. So the bandwidth of the power calculation is increased sequentially, which means that the dynamic performance is improved.

Details of the comparison of these methods are shown as Table 2. The accuracy and speed of method 1 are both the worst because of its low cut-off frequency. The accuracy of method 2 is the best because its result has no harmonics, but its response is not instantaneous. The response of the proposed method is the best, and its accuracy is also satisfactory. In addition, if the control precision is larger than the ripple of method 2, the influence of calculation ripple is constricted. The tradeoff comparison between power calculation accuracy and speed will be described in the following sections.

Table 2 Comparison of three power calculation methods

Method	Ripple	Speed	Complexity
1	Big	Slowest	Medium
2	Ripple free	Fast	Low
3	Small	Fastest	High

5 Performance comparison

The analysis of the three methods was verified by simulation results in MATLAB. First, we present the MATLAB calculation results of the three methods for a linear load and a non-linear load. Then, the simulation results of a wireless-parallel inverter system using each of the three methods are shown and compared.

5.1 Calculation results comparison

According to Eq. (16), the voltage is a sinusoidal waveform and the current has various odd harmonic components. Fig. 9 shows the voltage and current in linear load, and Fig. 10 shows them in non-linear load. For verifying the dynamic performance, the current changes at the times of 0.01 and 0.1 s.

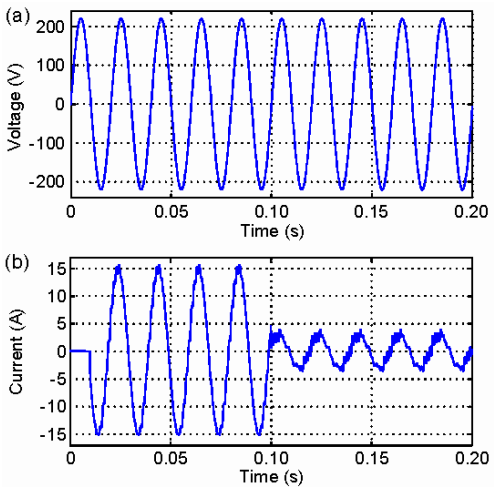

Fig. 9 Voltage (a) and current (b) in linear load

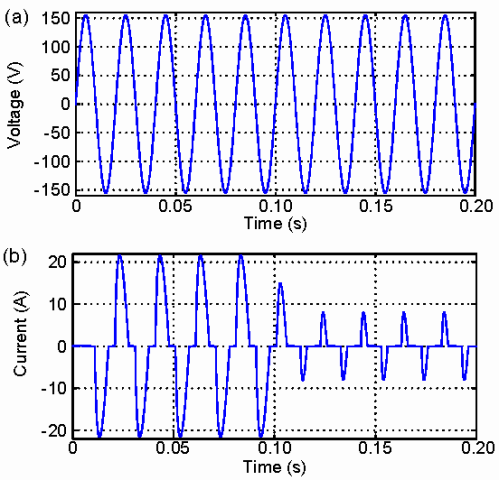

Fig.10 Voltage (a) and current (b) in non-linear load

When the load is linear, the active and reactive powers are as shown in Figs. 11 and 12, respectively. Figs. 11a and 11b show the results from method 1 in which the ω_c was set at 5 rad/s and 100 rad/s, respectively. Fig. 11c shows the results from method 2. Figs. 11d and 11e show the results from method 3 without and with an LPF in which ω_c was 100 rad/s, respectively. Fig. 12 is similar to Fig. 11.

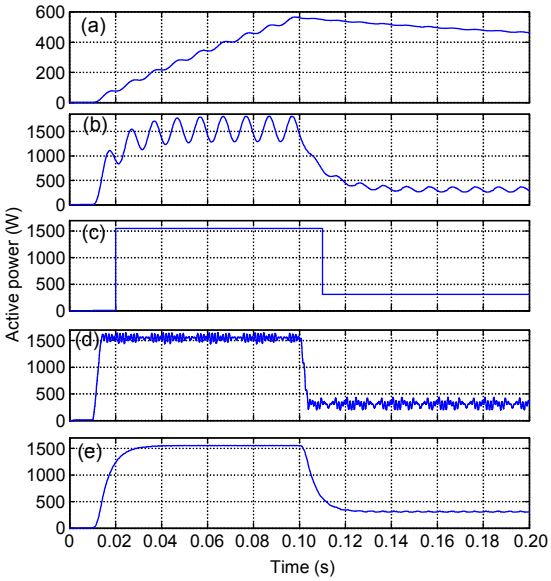

Fig. 11 Comparison of *P* calculation in linear load
(a) Method 1, ω_c=5 rad/s; (b) Method 1, ω_c=100 rad/s; (c) Method 2, without LPF; (d) Method 3, without LPF; (e) Method 3, ω_c=100 rad/s

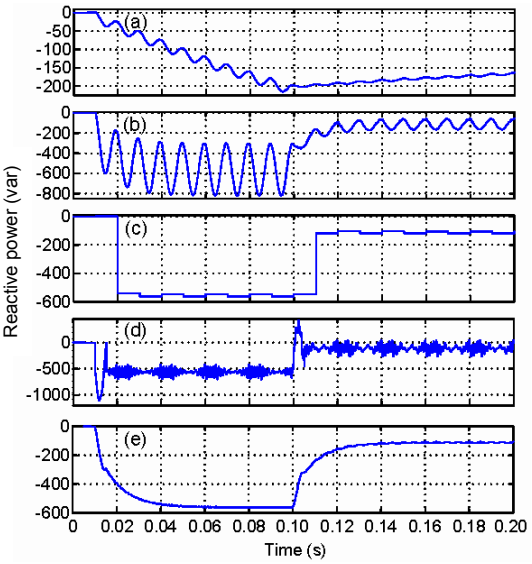

Fig. 12 Comparison of *Q* calculation in linear load
(a) Method 1, ω_c=5 rad/s; (b) Method 1, ω_c=100 rad/s; (c) Method 2, without LPF; (d) Method 3, without LPF; (e) Method 3, ω_c=100 rad/s

When the load is non-linear, the active and reactive powers are as shown in Figs. 13 and 14, respectively. The definition of cut-off frequency is the same as in Figs. 11 and 12.

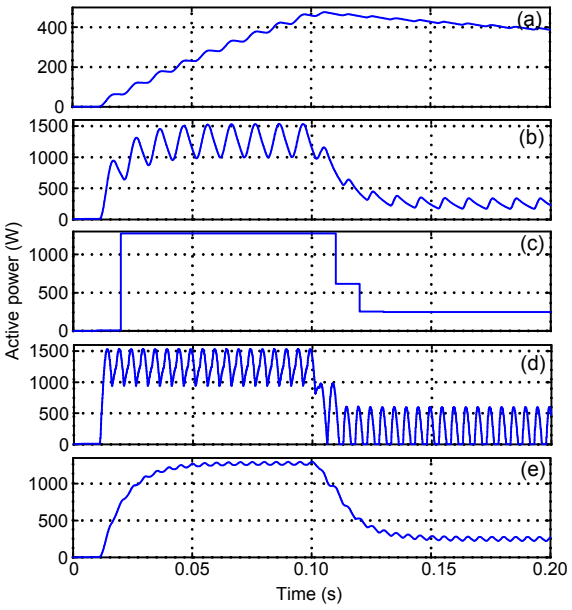

Fig. 13 Comparison of *P* calculation in non-linear load
(a) Method 1, ω_c=5 rad/s; (b) Method 1, ω_c=100 rad/s; (c) Method 2, without LPF; (d) Method 3, without LPF; (e) Methoud 3, ω_c=100 rad/s

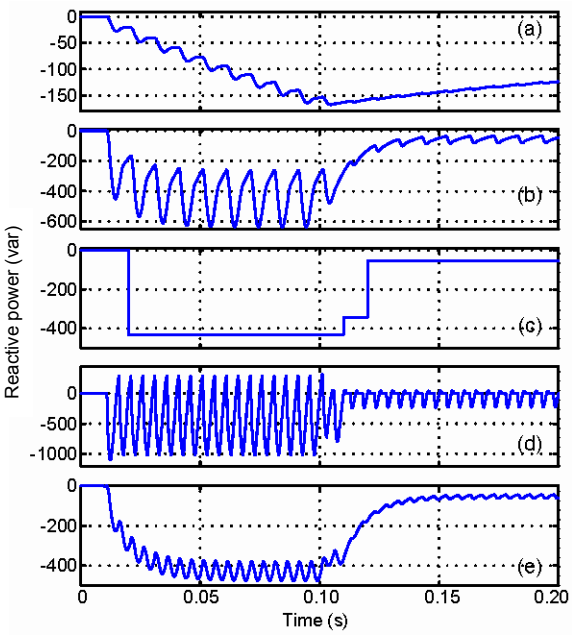

Fig. 14 Comparison of *Q* calculation in non-linear load
(a) Method 1, ω_c=5 rad/s; (b) Method 1, ω_c=100 rad/s; (c) Method 2, without LPF; (d) Method 3, without LPF; (e) Methoud 3, ω_c=100 rad/s

Comparing these figures, in method 1, an LPF with lower ω_c is necessary to obtain an accurate result, so its dynamic response is the slowest and its accuracy is not high. Method 2 has the highest accuracy and a very fast response, but in each cycle of 0.01 s it does nothing. It cannot fit sudden load-changes. Method 3 without an LPF has the fastest response to load changes, but its accuracy has some ripple and is not as good as that of method 2. Method 3 with an LPF represents a good tradeoff between accuracy and speed, achieving a good performance in power calculation.

5.2 Simulation of a parallel inverter system

To verify the performance of our proposed method, a simulation platform based on parallel inverters system was built on MATLAB and PLECS. In the platform, the whole control diagram of each inverter, including the sampling circuit, power calculation, droop method, and double-loop control, were realized in *Z*-domain and implemented with IQmath library of MATLAB, to simulate the digital control system behavior. The inverter's power stage was built with PLECS, which is a very powerful system-level simulation tool that can be integrated with MATLAB.

In the simulation platform, the circulating current is caused by the initial phase difference between the two inverter voltages. Then the circulating current is decreased by the conventional droop method. When using three different power calculation methods, the droop method performance will differ. In method 1, the cut-off frequency ω_c of the LPF was set to 10 rad/s for average active and reactive power calculations. In method 3, ω_c in *P* calculation was set to 200 rad/s, and ω_c in *Q* calculation was set to 100 rad/s. The simulation results are shown as follows.

The circulating currents using each of the three methods are shown in Fig. 15. The initial phase difference was set as 0.068 rad. The power calculation results are shown in Figs. 16–18.

The dynamic response of method 1 was the slowest, resulting in a settle time of about 900 ms. The accuracy of the active and reactive power calculations was the worst and its ripple was about 20 W.

The dynamic responses of methods 2 and 3 were similar. The settle times obtained from both methods were about 200 ms (Figs. 15b and 15c). However, the response of method 3 was faster than that of method 2

in the initial three periods. In Fig. 15c, the circulating current has decreased from 11.5 to 6 A in the second period. Nevertheless, in Fig. 15b, the circulating current has changed little in the second period. That is because method 3 can adjust the frequency and amplitude in every switching cycle, while method 2 can change them only once in each line-frequency period.

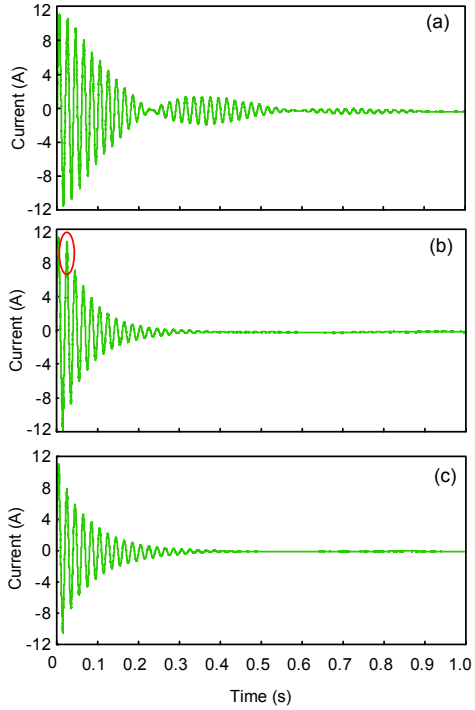

Fig. 15 Circulating current using methods 1 (a), 2 (b), and 3 (c)

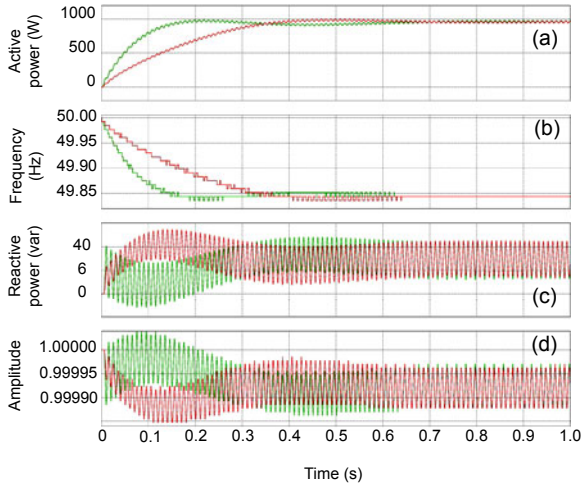

Fig. 16 Power calculation result using method 1
(a) Active power; (b) Frequency; (c) Reactive power; (d) Amplitude

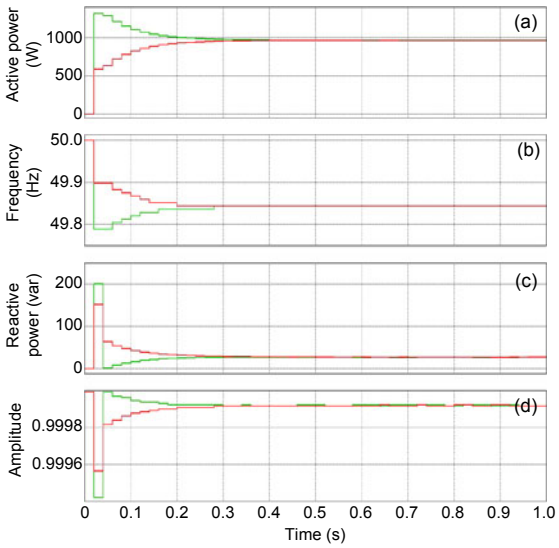

Fig. 17 Power calculation result using method 2
(a) Active power; (b) Frequency; (c) Reactive power; (d) Amplitude

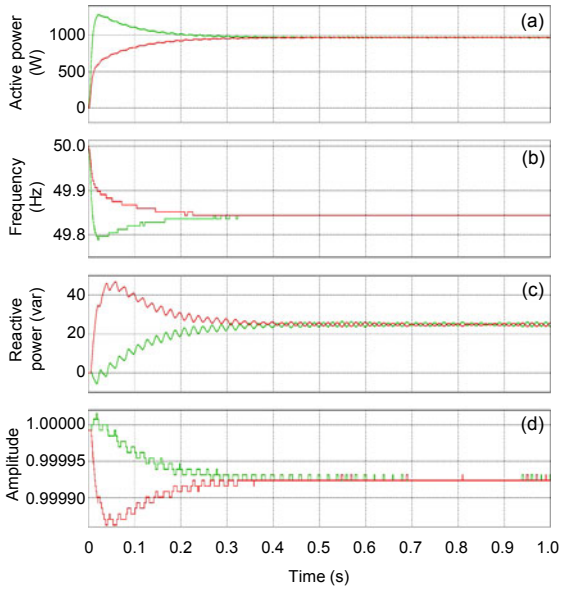

Fig. 18 Power calculation result using method 3
(a) Active power; (b) Frequency; (c) Reactive power; (d) Amplitude

Figs. 19 and 20 show details of the transient response of methods 2 and 3 in steady state, respectively. These figures confirm that the response of method 2 was periodic, and the response of method 3 was instantaneous. The resulting ripple of method 3 was still larger than that of method 2. However, since the control precision was larger than the ripples, its influence was very limited.

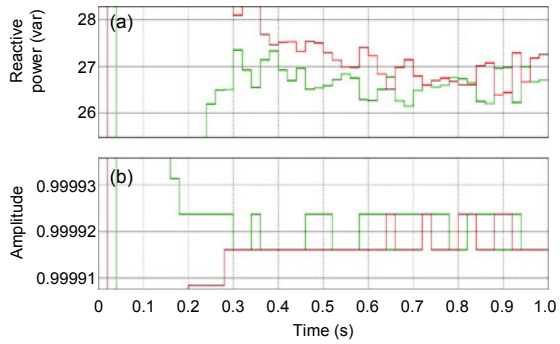

Fig. 19 Details of reactive power dynamics of method 2
(a) Reactive power; (b) Amplitude

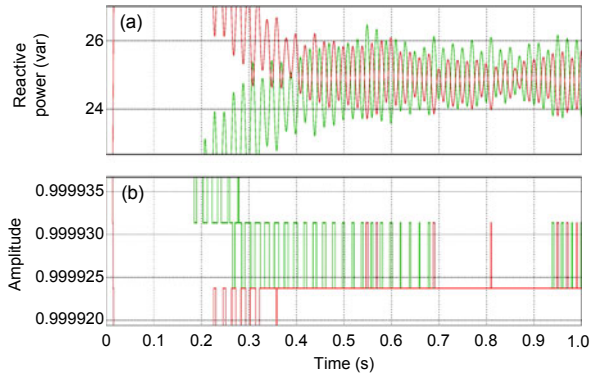

Fig. 20 Details of reactive power dynamics of method 3
(a) Reactive power; (b) Amplitude

6 Experimental results

A system including three 1-kW parallel inverters with 110 V/50 Hz voltage was implemented to simulate a stand-alone microgrid. This system was based on three inverter power stages of the Technology Dynamics Inc. (USA) (Fig. 21). Each inverter consisted of a single-phase IGBT full-bridge and an LC output filter. The control diagram including the droop control of the inverters was completely implemented using the DSP of TMS320F2808 (32-bit fixed-point 100 MHz) from the Texas Instruments (USA).

The experimental results of the parallel operation, for each of the three power calculation methods, are described below. The hardware and software was the same, except for the different power calculations, to provide a fair comparison.

One of the output currents was measured by a current transformer in the three-inverter system due to the lack of a measuring device. This may have distorted the experimental results when the current had odd harmonics, especially in the non-linear load condition.

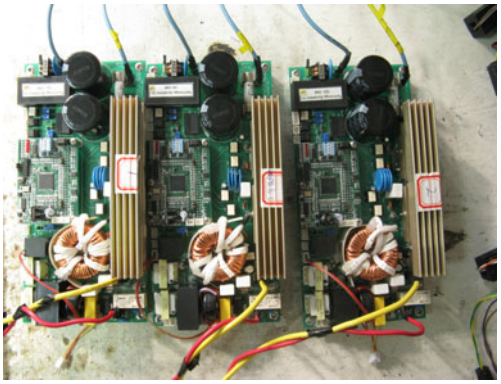

Fig. 21 The system with three 1-kW parallel inverters

6.1 Product & LPF method (method 1)

The results from the experiment using method 1 showed that a two-inverter system can work in a wireless parallel operation, but the system was not stable when supplying a linear load until the ω_c of the LPF was set to less than 10 rad/s (Fig. 22). This figure depicts the output current of one inverter at the moment of paralleling. The blue and pink traces are the output voltages (v_{o1} and v_{o2}) of two parallel inverters, and the green trace is the output current i_{o1} of one inverter.

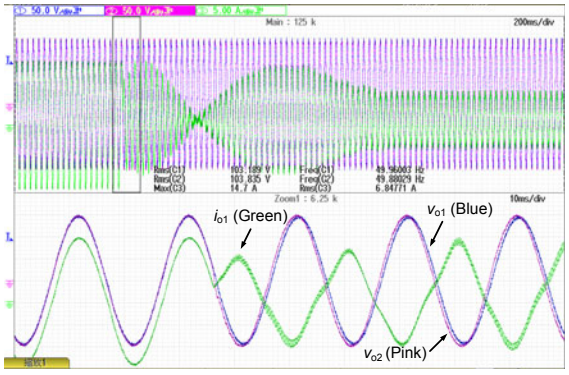

Fig. 22 Dynamic response of a two-inverter system using method 1

From Fig. 22, the settle time was about 50 periods. At the beginning of the parallel operation, there was a very large inrush circulating current. The phase of the output current was 180° delayed with respect to

the output voltage, which means that this inverter delivered reactive power to the common load. This situation is bad for a parallel operation.

Fig. 23 shows the dynamic response of the three-inverter system: the parallel operation failed when the load changed from non-load to full load. This figure also proves the weak performance of method 1.

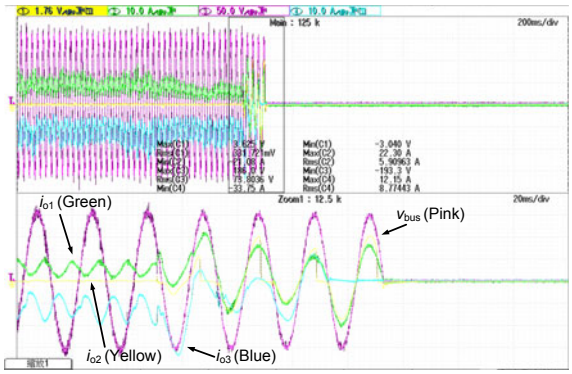

Fig. 23 Dynamic response of a three-inverter system using method 1

6.2 Period-average method (method 2)

The performance of method 2 was proved in a three-inverter system when the load changed from non-load to full load. Figs. 24a and 24b depict the dynamic response when supplying linear and non-linear loads, respectively, showing that the settle time was still about two or three periods. There was still a visible inrush circulating current at the beginning of the parallel operation, which caused voltage distortion.

6.3 Proposed method (method 3)

In the experiment using method 3, the cut-off frequency was set to 100 rad/s. Figs. 25a and 25b show the output currents for the three-inverter system when the load changed. The load was linear in Fig. 25a and non-linear in Fig. 25b. These figures show that the settle time for method 3 was about one period. The inrush circulating current was suppressed for linear or non-linear loads. However, voltage distortion was still present at the beginning of the parallel operation. Figs. 26a and 26b show the steady-state currents for method 3 using linear and non-linear loads, respectively, in a two-inverter system, and Figs. 27a and 27b show the steady state in a three-inverter system for the same load conditions.

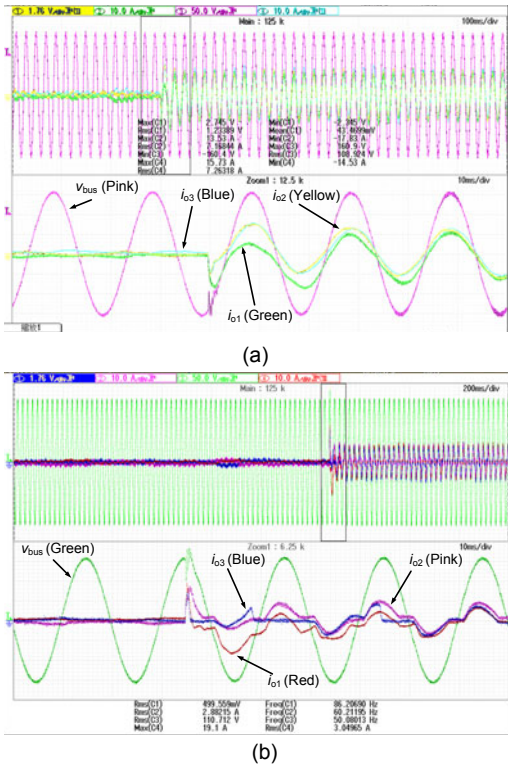

Fig. 24 Dynamic response in linear load (a) and non-linear load (b) using method 2

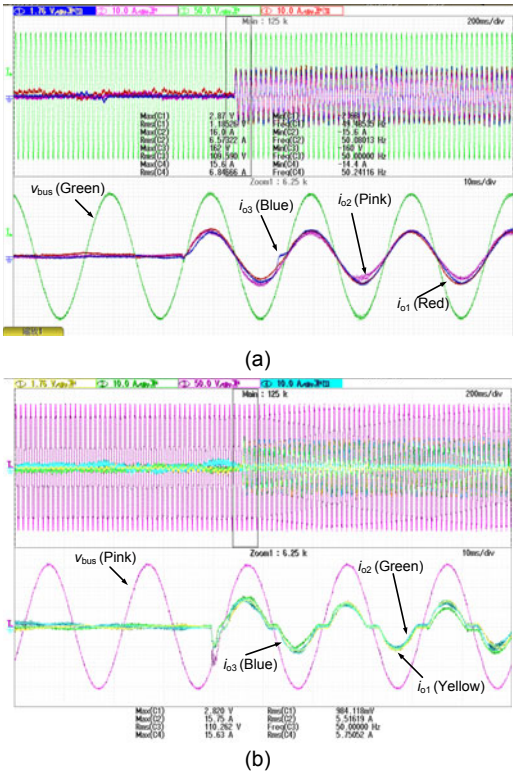

Fig. 25 Dynamic response in linear load (a) and non-linear load (b) using method 3 in a three-inverter system

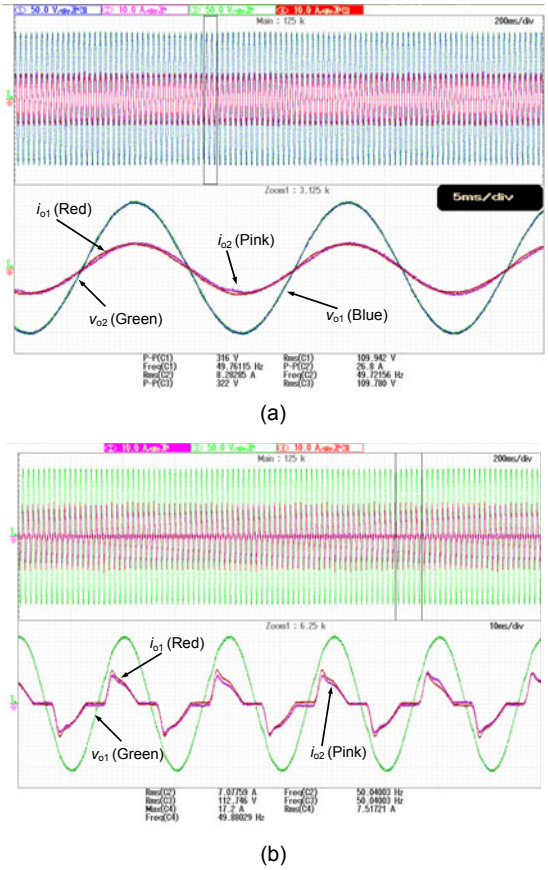

Fig. 26 Steady state in linear load (a) and non-linear load (b) using method 3 in a two-inverter system

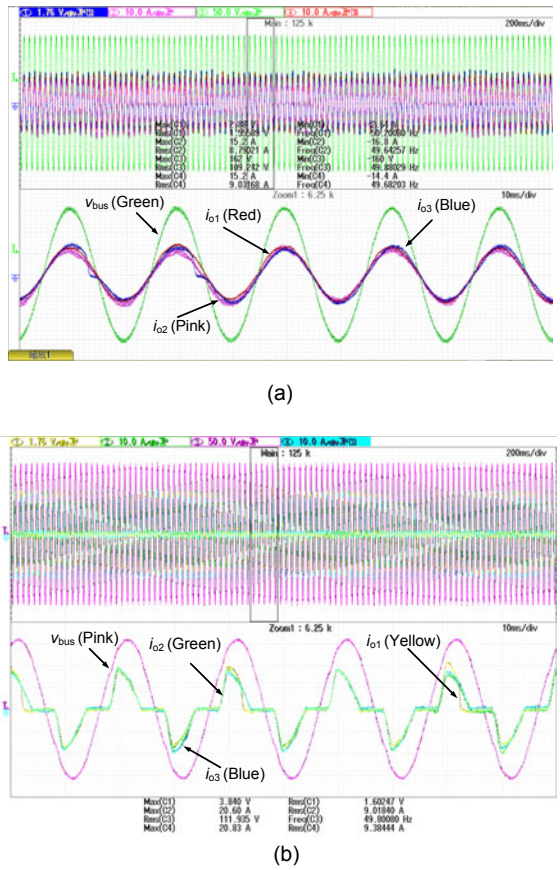

Fig. 27 Steady state in linear load (a) and non-linear load (b) using method 3 in a three-inverter system

The results of these comparisons show that the proposed method based on *p-q* theory presents the best dynamic response and steady-state performance. This method presents a good balance between accuracy and speed in the power calculation process.

7 Conclusions

A parallel operation using a droop method without inter-communications is an attractive solution for islanded microgrids. This paper focuses on the digital implementation of the droop method in DSP platforms. The performance of the digital control system is important in droop method implementation, according to our analysis. However, many of the leading droop methods include complicated algorithms, which present problems for digital control systems. Thus, the choice of method for implementing the control loop is very important for the performance of the droop method.

In the implementation of the droop method, the power calculation is a very critical aspect for the load sharing of the parallel system, because it is the bottleneck for achieving a good circulating current dynamic response and good accuracy to guarantee steady-state performance. Thus, this paper deals with improving the performance of the droop method by improving the power calculation method. A power calculation based on the modified instantaneous *p-q* theory is proposed.

Compared with traditional methods, our proposed method needs an LPF to obtain accurate values of P and Q. However, the power calculation is still fast enough because the cut-off frequency is so high. The response of the method is very fast, which can improve the dynamic performance of a parallel operation in load changing. However, this algorithm is the most complex and needs more memory space to delay voltage and current by 90°. This has to be considered in the algorithm's optimization. Finally, simulation and experimental results are presented from a

MATLAB/PLECS platform and a system composed of three 1-kW parallel inverters using a DSP with droop control. The results validate the performance of our proposed power calculation method.

References

Afonso, J.L., Freitas, M.J.S., Martins, J.S., 2003. *p-q* Theory Power Components Calculations. IEEE Int. Symp. on Industrial Electronics, **1**:385-390. [doi:10.1109/ISIE.2003.1267279]

Ahn, S.J., Park, J.W., Chung I.Y., Moon S.I., Kang, S.H., Nam, S.R., 2010. Power-sharing method of multiple distributed generators considering control modes and configurations of a microgrid. *IEEE Trans. Power Del.*, **25**(3):2007-2016. [doi:10.1109/TPWRD.2010.2047736]

Aredes, M., Akagi, H., Watanabe, E.H., Vergara Salgado, E., Encarnacao, L.F., 2009. Comparisons between the *p-q* and *p-q-r* theories in three-phase four-wire systems. *IEEE Trans. Power Electr.*, **24**(3-4):924-933. [doi:10.1109/TPEL.2008.2008187]

Barklund, E., Pogaku, N., Prodanovic, M., Hernandez-Aramburo, C., Green, T.C., 2008. Energy management in autonomous microgrid using stability constrained droop control of inverters. *IEEE Trans. Power Electr.*, **23**(5):2346-2352. [doi:10.1109/TPEL.2008.2001910]

Chiang, S.J., Yen, C.Y., Chang, K.T., 2001. A multimodule parallelable series-connected PWM voltage regulator. *IEEE Trans. Ind. Electr.*, **48**(3):506-517. [doi:10.1109/41.925577]

Chung, I.Y., Liu, W., Cartes, D.A., Collins, E.G., Moon S.I., 2010. Control methods of inverter-interfaced distributed generators in a microgrid system. *IEEE Trans. Ind. Appl.*, **46**(3):1078-1088. [doi:10.1109/TIA.2010.2044970]

de Brabandere, K., Bolsens, B., van den Keybus, J., Woyte, A., Driesen, J., Belmans, R., 2007. A voltage and frequency droop control method for parallel inverters. *IEEE Trans. Power Electr.*, **22**(4):1107-1115. [doi:10.1109/TPEL.2007.900456]

Diaz, G., Gonzalez-Moran, C., Gomez-Aleixandre, J., Diez, A., 2010. Scheduling of droop coefficients for frequency and voltage regulation in isolated microgrids. *IEEE Trans. Power Syst.*, **25**(1):489-496. [doi:10.1109/TPWRS.2009.2030425]

Golestan, S., Joorabian, M., Rastegar, H., Roshan, A., Guerrero, J.M., 2009. Droop Based Control of Parallel-Connected Single-Phase Inverters in *d-q* Rotating Frame. IEEE Int. Conf. Industrial Technology, p.1-6. [doi:10.1109/ICIT.2009.4939564]

Guerrero, J.M., de Vicuna, L.G., Matas, J., Castilla, M., Miret, J., 2004. A wireless controller to enhance dynamic performance of parallel inverters in distributed generation systems. *IEEE Trans. Power Electr.*, **19**(5):1205-1213. [doi:10.1109/TPEL.2004.833451]

Guerrero, J.M., Garciade Vicuna, L., Matas, J., Castilla, M., Miret, J., 2005. Output impedance design of parallel-connected UPS inverters with wireless load-sharing control. *IEEE Trans. Ind. Electr.*, **52**(4):1126-1136. [doi:10.1109/TIE.2005.851634]

Guerrero, J.M., Matas, J., de Vicuna, L.G., Castilla, M., Miret, J., 2006. Wireless-control strategy for parallel operation of distributed generation inverters. *IEEE Trans. Ind. Electr.*, **53**(5):1461-1470. [doi:10.1109/TIE.2006.882015]

Guerrero, J.M., Hang, L., Uceda, J., 2008. Control of distributed uninterruptible power supply systems. *IEEE Trans. Ind. Electr.*, **55**(8):2845-2860. [doi:10.1109/TIE.2008.924173]

Guerrero, J.M., Vasquez, J.C., Matas, J., Castilla, M., de Vicuna, L.G., 2009. Control strategy for flexible microgrid based on parallel line-interactive UPS systems. *IEEE Trans. Ind. Electr.*, **36**(3):726-736. [doi:10.1109/TIE.2008.2009274]

Guerrero, J.M., Blaabjerg, F., Zhelev, T., Hemmes, K., Monmasson, E., Jemei, S., Comech, M.P., Granadino, R., Frau, J.I., 2010. Distributed generation: toward a new energy paradigm. *IEEE Ind. Electr. Mag.*, **4**(1):52-64. [doi:10.1109/MIE.2010.935862]

Hasanzadeh, A., Onar, O.C., Mokhtari, H., Khaligh, A., 2010. A proportional-resonant controller-based wireless control strategy with a reduced number of sensors for parallel-operated UPSs. *IEEE Trans. Power Del.*, **25**(1):468-478. [doi:10.1109/TPWRD.2009.2034911]

Hatziargyriou, N., Asano, H., Iravani, R., Marnay, C., 2007. Microgrids. *IEEE Power Energy Mag.*, **5**(4):78-94. [doi:10.1109/MPAE.2007.376583]

He, J., Li, Y.W., 2011. Analysis, design, and implementation of virtual impedance for power electronics interfaced distributed generation. *IEEE Trans. Ind. Appl.*, **47**(6):2525-2539. [doi:10.1109/TIA.2011.2168592]

Kroposki, B., Lasseter, R., Ise, T., Morozumi, S., Papatlianassiou, S., Hatziargyriou, N., 2008. Making microgrids work. *IEEE Power Energy Mag.*, **6**(3):40-53. [doi:10.1109/MPE.2008.918718]

Li, Y.W., Kao, C.N., 2009. An accurate power control strategy for power-electronics-interfaced distributed generation units operating in a low-voltage multi-bus microgrid. *IEEE Trans. Power Electr.*, **24**(12):2977-2988. [doi:10.1109/TPEL.2009.2022828]

Majumder, R., Chaudhuri, B., Ghosh, A., Majumder, R., Ledwich, G., Zare, F., 2010. Improvement of stability and load sharing in an autonomous microgrid using supplementary droop control loop. *IEEE Trans. Power Syst.*, **25**(2):796-808. [doi:10.1109/TPWRS.2009.2032049]

Marwali, M.N., Jung, J.W., Keyhani, A., 2004. Control of distributed generation systems-part II: load sharing control. *IEEE Trans. Power Electr.*, **19**(6):1551-1561. [doi:10.1109/TPEL.2004.836634]

Matas, J., Castilla, M., de Vicuña, L.G., Miret, J., Vasquez, J.C., 2010. Virtual impedance loop for droop-controlled single-phase parallel inverters using a second-order general-integrator scheme. *IEEE Trans. Power Electr.*, **25**(12):2993-3003. [doi:10.1109/TPEL.2010.2082003]

Mohamed, Y., El-Saadany, E.F., 2008. Adaptive decentralized droop controller to preserve power sharing stability of paralleled inverters in distributed generation microgrids.

IEEE Trans. Power Electr., **23**(6):2806-2816. [doi:10.1109/TPEL.2008.2005100]

Oliveira da Silva, S.A., Novochadlo, R., Modesto, R.A., 2008. Single-Phase PLL Structure Using Modified *p-q* Theory for Utility Connected Systems. IEEE Power Electronics Specialists Conf., p.4706-4711. [doi:10.1109/PESC.2008.4592712]

Ren, Z., Gao, M., Mo, Q., Liu, K., Yao, W., Chen, M., Qian, Z., 2010. Power Calculation Method Used in Wireless Parallel Inverters under Nonlinear Load Conditions. 25th Annual IEEE Conf. and Expo. on Applied Power Electronics, p.1674-1677. [doi:10.1109/APEC.2010.5433456]

Rokrok, E., Golshan, M.E.H., 2010. Adaptive voltage droop scheme for voltage source converters in an islanded multibus microgrid. *IET Gener. Transm. Distr.*, **4**(5):562-578. [doi:10.1049/iet-gtd.2009.0146]

Roslan, A.M., Ahmed, K.H., Finney, S.J., Williams, B.W., 2011. Improved instantaneous average current-sharing control scheme for parallel-connected inverter considering line impedance impact in microgrid networks. *IEEE Trans. Power Electr.*, **26**(3):702-716. [doi:10.1109/TPEL.2010.2102775]

Sun, X., Lee, Y.S., Xu, D., 2003. Modeling, analysis, and implementation of parallel multi-inverter systems with instantaneous average current sharing scheme. *IEEE Trans. Power Electr.*, **18**(3):844-856. [doi:10.1109/TPEL.2003.810867]

Yang, S.Y., Zhang, C.W., Zhang, X., Cao, R.X., Shen, W.X., 2006. Study on the Control Strategy for Parallel Operation of Inverters Based on Adaptive Droop Method. IEEE Conf. on Industrial Electronics and Applications, p.1-5. [doi:10.1109/ICIEA.2006.257292]

Yao, W., Gao, M., Ren, Z., Chen, M., Qian, Z., 2010. Study on the Impact of the Complex Impedance on the Droop Control Method for the Parallel Inverters. Applied Power Electronics Conf. and Expo., p.1204-1208. [doi:10.1109/APEC.2010.5433348]

Yao, W., Chen, M., Matas, J., Guerrero, J.M., Qian, Z., 2011. Design and analysis of the droop control method for parallel inverters considering the impact of the complex impedance on the power sharing. *IEEE Trans. Ind. Electr.*, **58**(2):576-588. [doi:10.1109/TIE.2010.2046001]